Int. J. Heat Mass Transfer. Vol. 36, No. 2, pp. 489–505, 1993
Printed in Great Britain

0017-9310/93 $6.00 + 0.00

Effect of rotation on fluid motion and channel formation during unidirectional solidification of a binary alloy

D. G. NEILSON and F. P. INCROPERA

Heat Transfer Laboratory, School of Mechanical Engineering, Purdue University, West Lafayette, IN 47907, U.S.A.

(*Received* 18 *September* 1991 *and in final form* 16 *January* 1992)

Abstract—When off-eutectic binary alloys are cast by means of unidirectional solidification (UDS), perturbations in density and permeability along the liquidus front may result in the nucleation and subsequent growth of vertical flow channels in the two-phase (solid/liquid) mushy region. The channels subsequently become locations of severe compositional nonhomogeneity which are commonly termed freckles. In this study UDS of hypereutectic NH_4Cl–H_2O has been numerically simulated to determine the effects of both steady and intermittent mold rotation. For slow, steady rotation up to 120 rpm, it was found that related inertial effects were insufficient to significantly alter buoyancy induced mechanisms responsible for channel formation. However, for intermittent rotation corresponding to successive *spin-up* and *spin-down* of the mold, channel nucleation was confined to the centerline and outer radius of the casting. The elimination of channels from the core of the casting is attributed to the impulsive change in angular frequency associated with spin-up and its effect on establishing an Ekman layer along the liquidus front. The front is *washed* by flow within the layer, thereby eliminating the perturbations responsible for channel nucleation.

1. INTRODUCTION

PHASE transformation during solidification of an off-eutectic binary solution occurs over a range of temperatures, the extremes of which are prescribed by the liquidus and solidus temperatures of the solution. At temperatures intermediate to these extremes, the solution is characterized by co-existing solid and liquid phases in what is commonly termed a *mushy zone*. For many commercially important metal alloys, the morphology of the mushy zone is characterized by a solid–liquid porous structure, with solid phase crystals in the form of dendrites.

An important feature of solidification in the mushy region pertains to rejection of one of the chemical constituents into the liquid. Solute rejection induces species composition gradients which, in combination with existing temperature gradients and a gravitational field, may induce buoyancy driven convection in the mush and the parent melt. If the solutal and thermal gradients make opposing contributions to the hydrodynamic stability of the system, the convection may be double-diffusive, yielding horizontal layers or vertical fingers, according to whether the temperature or the composition field is destabilizing [1]. The redistribution of chemical species due to convection is responsible for a condition known as *macrosegregation*, which refers to the existence of large-scale species inhomogeneities in the final casting. Regions of pronounced variations in composition significantly diminish the quality of an alloy casting and are termed *segregates* [2].

A particularly severe form of macrosegregation is associated with *unidirectional solidification* (UDS), wherein solidification progresses upward in a binary melt which is chilled from below. If the lighter constituent is rejected as solidification occurs in the mushy zone, the accompanying density inversion may become unstable, leading first to double-diffusive convection characterized by alternating fingers of compositionally lighter and heavier fluid ascending from and descending to the liquidus interface, respectively [3]. Such fluid motion is a precursor to the formation of vertical flow channels within the mushy region and ultimately to the formation of *freckle* segregates, which are vertically aligned regions of nearly eutectic composition in the final casting. During solidification, plumes emanating from the channels induce large-scale convection in the melt.

Copley *et al.* [4] and Giamei and Kear [5] were the first to recognize the presence and role of double-diffusive convection in the freezing of bottom-chilled castings. In both aqueous NH_4Cl, a metal analog that freezes dendritically, and nickel-based superalloys, freckle segregates could be traced to fluid motion induced by a density inversion.

Morphological and convection instabilities associated with UDS have been analyzed [6–13], and useful insights have been obtained. For example, Heinrich *et al.* [12] have confirmed that, pursuant to convective instability, motion within the melt is characterized by finger-like double-diffusive convection, which entrains interdendritic liquid adjoining the liquidus front, thereby influencing local solute concentrations. The results provide the first predicted evidence that variations in field variables along the liquidus front

NOMENCLATURE

c	specific heat
D	binary mass diffusivity
E	Ekman number, $\nu/\omega H^2$
f	mass fraction
g	volume fraction or gravitational acceleration
h	enthalpy
H	axial height of computational domain
k	thermal conductivity
P	pressure
r	radial coordinate
r_0	radius of computational domain
t	time
T	temperature
u	radial velocity component
v	circumferential velocity component
w	axial velocity component
$\mathbf{V}$	velocity vector
z	axial coordinate.

Greek symbols

β_S	solutal volumetric expansion coefficient
β_T	thermal volumetric expansion coefficient
θ	circumferential direction
κ	permeability
κ_0	Blake–Kozeny permeability constant
μ	dynamic viscosity
ν	kinematic viscosity
ρ	density
$\bar{\rho}_s$	partial density of solid phase
χ	spin-up time
ω	angular frequency
Ω	swirl.

Subscripts

0	initial
c	cold wall
e	eutectic
l	liquid
s	solid.

Superscripts

α	species designation
*	normalized variable.

may initiate localized remelting and freckle segregate formation. However, the calculations only pertain to the onset of convection, since the liquid volume fraction of the mushy region, which strongly influences results, was treated as a constant.

To compute, in detail, events which precede and follow the onset of convection, it is necessary to employ models which can track the development of liquidus and solidus interfaces and which can accommodate the complex interactions between mass, momentum, energy and species transfer in the melt and mushy regions. To date, the most comprehensive approaches to numerical simulation of binary solidification have involved continuum and volume-averaging formulations of the macroscopic conservation equations [14–17]. Although slightly different in their development, these approaches yield similar finalized forms of the conservation equations [18]. Initial simulations considered solidification from the chilled side wall of a mold and were successful in predicting important phenomena such as remelting due to liquidus temperature depression, the influence of interdendritic flow on the development of segregates, liquidus front irregularities, and double-diffusive layering in the melt [16, 19–21]. More recently, the model has been used to predict details associated with channel and freckle formation in UDS. From a two-dimensional (r–z) simulation of UDS in a cylindrical mold [22], channel growth was predicted to begin at the liquidus front and, due to localized melting, to propagate downward toward the chill plate. The channels were predicted to provide paths of least resistance for transport of interdendritic fluid into the overlying melt and to provide sites for subsequent freckle formation. From a fully three-dimensional (r, θ, z) simulation [23, 24], the *pencil-like* nature of the channels and freckles has been predicted.

Because of the deleterious effects of freckling, measures for inhibiting fluid motion in UDS have been investigated. From experiments performed in an alternating increasing–decreasing g field (produced by parabolic trajectories in an aircraft), plumes issuing from a solidfying aqueous NH_4Cl alloy were completely suppressed during low-g conditions [25]. In an experiment designed to eliminate freckles, Sample and Hellawell [26, 27] employed a rotation/tilting technique to alter the orientation of gravity relative to a chilled bottom surface, at which solidification was induced in a cylindrical mold containing aqueous NH_4Cl. For slow, steady rotation of the mold about the vertical (no tilting), freckle development was essentially identical to that of the static case, for which channels developed in a seemingly random pattern within the mush. However, for slow, steady rotation of a tilted mold, the number of freckles was dramatically reduced or, for some conditions, completely eliminated. Although it was originally hypothesized that mold rotation would inhibit channel formation by preventing sustained interdendritic flow in a single direction, it was ultimately concluded that the

decrease in freckles was due primarily to bulk liquid translation across the liquidus front. Such translation was believed to eliminate perturbations related to boundary layer growth at the liquidus front, before the perturbations could grow and become unstable. An implication of this explanation is that bulk liquid agitation may be a viable means of preventing freckle formation.

With the exception of the foregoing studies [25–27], little has been done to consider means by which freckling may be inhibited by altering interdendritic flows associated with UDS. One option, which is readily implemented for a cylindrical mold, involves the use of mold rotation to impose a centrifugal force on the flow. The objective of this study has been to numerically simulate the effect of such a body force for both steady and intermittent rotation of a cylindrical mold and to assess its influence on freckling by comparing results with those previously obtained for static solidification [22].

2. MATHEMATICAL MODEL

Unidirectional solidification of a binary solution in a vertical, cylindrical cavity which is chilled from below and rotated about its axis has been simulated using a continuum model which incorporates all pertinent macroscopic transport phenomena in the governing equations [14, 18]. The model is based on the following postulates of mixture theory: (i) phases may be treated as isolated subsystems, if mutual interactions are properly accommodated; (ii) mixture properties may be mathematically represented in terms of individual phase properties; and (iii) the mean collective mixture behavior may be described by equations which are analogous to those governing the individual phases. Using these postulates and assuming (i) axial symmetry (two-dimensional conditions in r and z), (ii) equivalent phase densities ($\rho_s = \rho_l = \rho$), and (iii) use of Darcy's law to represent solid–liquid drag forces in an isotropic mushy region, the continuum conservation equations for mass, momentum, energy and species transfer, respectively, may be expressed as [23]

$$\frac{\partial \rho}{\partial t} + \nabla \cdot (\rho \mathbf{V}) = 0 \tag{1}$$

$$\frac{\partial}{\partial t}(\rho u) + \nabla \cdot (\rho \mathbf{V} u) = \nabla \cdot (\mu \nabla u) - \frac{\mu}{r^2}(u - f_s u_s) - \frac{\partial P}{\partial r} - \frac{\mu}{\kappa}(u - u_s) + \frac{\rho_l v_l^2}{r} + \frac{D}{Dt}(\bar{\rho}_s u_s) \tag{2}$$

$$\frac{\partial}{\partial t}(\rho w) + \nabla \cdot (\rho \mathbf{V} w) = \nabla \cdot (\mu \nabla w) - \frac{\partial P}{\partial z} - \frac{\mu}{\kappa}(w - w_s) - \rho_l g + \frac{D}{Dt}(\bar{\rho}_s w_s) \tag{3}$$

$$\frac{\partial}{\partial t}(\rho h) + \nabla \cdot (\rho \mathbf{V} h) = \nabla \cdot \left(\frac{k}{c_s} \nabla h\right) + \nabla \cdot \left(\frac{k}{c_s}(h_s - h)\right) - \nabla \cdot \left(\rho \frac{f_s}{f_l}(\mathbf{V} - \mathbf{V}_s)(h - h_s)\right) \tag{4}$$

$$\frac{\partial}{\partial t}(\rho f^{\alpha}) + \nabla \cdot (\rho \mathbf{V} f^{\alpha}) = \nabla \cdot (\rho D \nabla f^{\alpha}) + \nabla \cdot (\rho D \nabla (f_l^{\alpha} - f^{\alpha})) - \nabla \cdot \left(\rho \frac{f_s}{f_l}(\mathbf{V} - \mathbf{V}_s)(f^{\alpha} - f_s^{\alpha})\right). \tag{5}$$

where α refers to one of the two mixture components and continuum variables such as ρ, $\mathbf{V}$, and h are defined on the basis of mean mixture theory [14, 18].

Each of the foregoing equations was developed by summing individual phase conservation relations to obtain continuum quantities as dependent variables, as well as terms involving phase specific quantities. Equation (2), for example, is a conservation statement for the radial momentum of the mixture, which may be applied in all regions (solid, liquid, and mushy) of the domain. The terms on the left side of equation (2) represent the time rate of change of radial momentum within a differential volume and the net advection of radial momentum to the differential volume. The first two terms on the right side of the equation account for radial momentum changes associated with viscous effects, while the third term accounts for momentum changes due to a radial pressure gradient. The fourth term on the right side accommodates liquid–solid interactions in the porous mushy region through Darcy's law, and the fifth term accounts for the centripetal force associated with rotation. The final (solid phase acceleration) term accounts for a portion of the solid stress variation [18]. Except for replacement of the centripetal acceleration by the body force due to gravity, similar terms characterize the axial momentum equation (3).

The influence of thermally and solutally induced buoyancy is accommodated by prescribing a variable liquid density, ρ_l, in the gravitational term and by using the Bousinesq approximation to represent the effects of temperature, T, and liquid composition, f_l^{α}. Hence

$$\rho_l = \rho_{l,0} + \rho_{l,0}[\beta_T (T - T_0) + \beta_S (f_l^{\alpha} - f_{l,0}^{\alpha})] \tag{6}$$

where the subscript 0 refers to reference conditions. To properly account for the combined effects of rotation and density stratification due to phase change, equation (6) was also used to evaluate ρ_l in the centripetal acceleration term of equation (2).

To investigate the effects of rotation under the assumption of two-dimensional (axisymmetric) behavior, the circumferential velocity v must be determined. The centripetal acceleration, which is based on v, links the effects of rotation to momentum production in the radial direction. Although a circumferential momentum equation could be used to

obtain the radial and axial dependence of v, the Coriolis term which appears in this equation is known to become computationally troublesome for large, negative radial velocities that may occur near the centerline [28]. To circumvent this difficulty, a conservation equation for angular momentum per unit mass, $\Omega = rv$, which is often called the swirl, may be used [29].

An expression for the conservation of swirl for a particular phase may be obtained by forming the vector cross product of the radial position vector $\mathbf{r}$ and the equation for conservation of linear momentum in the circumferential direction. Summing the individual phase equations and introducing mixture properties, the following form of the continuum swirl equation may be obtained [23]:

$$\frac{\partial}{\partial t}(\rho\Omega)+\nabla\cdot(\rho\mathbf{V}\Omega)=\nabla\cdot(\mu\nabla\Omega)-\frac{2\mu}{r}\frac{\partial\Omega}{\partial r}-\frac{\mu}{\kappa}(\Omega-\Omega_s)$$

$$-\nabla\cdot\left(\rho\frac{f_s}{f_l}(\mathbf{V}-\mathbf{V}_s)(\Omega-\Omega_s)\right)+\frac{D}{Dt}(\bar{\rho}_s\Omega_s) \quad (7)$$

where Ω is the continuum swirl

$$\Omega = f_s\Omega_s + f_l\Omega_l. \quad (8)$$

To complete the mathematical model, phase equilibrium is assumed and the phase diagram of the mixture is used to relate the local enthalpy and temperature and to evaluate phase mass fractions and compositions. Closure relations based on the equilibrium phase diagram are provided elsewhere [23, 30]. In addition, since the solid phase is assumed to be rigid and continuous, component velocities of $u_s = w_s = 0$ are associated with the radial and axial directions, respectively, while the circumferential component, v_s, is determined by the prescribed angular frequency of the rotation.

The isotropic permeability appearing in equations (2), (3) and (7) is assumed to depend only on the liquid volume fraction and to be determined by the empirical Blake–Kozeny equation

$$\kappa = \kappa_0\frac{g_l^3}{(1-g_l)^2}. \quad (9)$$

The constant κ_0 depends on the morphology of the mushy region and may be linked to primary/secondary dendrite arm spacings [DAS]. For the solidification system of interest in this study (NH_4Cl–H_2O), a value of $\kappa_0 = 5.5\times10^{-12}$ m^2 was assumed, which corresponds to a DAS of approximately 32 μm [23, 31]. Thermophysical properties of the NH_4Cl–H_2O system were assumed to be constant, with values corresponding to those previously used to simulate a static casting [22].

The conservation equations were solved using a control-volume based, finite-difference scheme [30, 32]. To permit a comparison of results with those previously obtained for a static casting [22], the height and radius of the cylindrical mold were fixed at $H = 102$ mm and $r_0 = 64$ mm, respectively. To assess grid independence, calculations were performed for biased 42×42, 66×66 and 82×82 grids. The 66×66 grid (Fig. 1) provided sufficient detail to resolve all salient features obtained from the 82×82 grid and also predicted global quantities, such as heat rate and solid mass formation, which were in excellent agreement with predictions based on the finer grid. Results were also compared with those obtained from a fully three-dimensional simulation, and apart from being unable to predict the actual, pencil-like nature of the channeling/freckling phenomena, the two-dimensional simulation yielded all other key features of the solidification process, as well as global quantities which were in good agreement with the three-dimensional results [23, 24].

For the linear and angular momentum equations, no-slip conditions were prescribed at the bottom ($z = 0$), vertical ($r = r_0$), and top ($z = H$) surfaces of the mold. The vertical and top surfaces were treated as adiabatic, while the bottom was maintained at a uniform chill temperature, T_c. The swirl was specified along all bounding surfaces according to the prescribed angular frequency ($\Omega = vr = \omega r^2$). Symmetry conditions were imposed at the centerline, and all boundaries were rendered impermeable to species transfer.

To be consistent with previous simulations for a static casting [22], calculations were performed for a binary melt of initial composition and temperature equal to $f_0^{NH_4Cl} = 0.32$ and $T_0 = 50$°C, respectively. The initial composition, which exceeds the eutectic

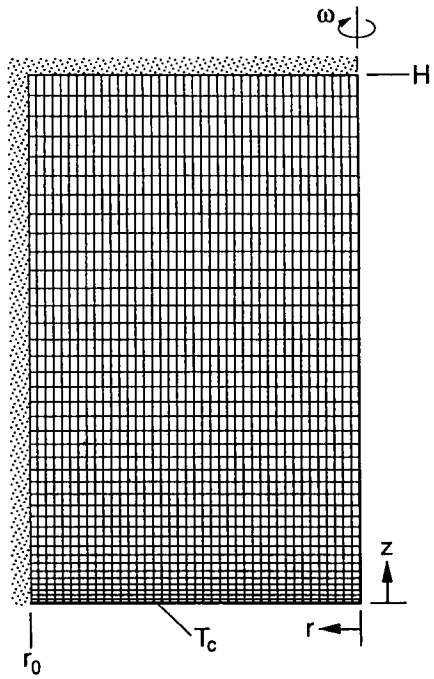

FIG. 1. Two-dimensional representation of mold geometry with computational grid.

value of $f_e^{NH_4Cl} = 0.197$, provides for extensive mushy region development and release of the lighter component (H_2O) during solidification. Solidification was initiated by imposing a chilled bottom temperature of -14 C, which slightly exceeds the eutectic temperature of -15.4 C.

Time step independence was achieved by using an increment of $\Delta t = 1$ s, with up to 70 iterations needed for convergence. The calculations were performed using Gould NP/1 and DEC VAX8800 computers, with approximately 25 CPU seconds required per iteration.

3. RESULTS

Predictions of this study for steady and intermittent rotation will be contrasted with those previously reported for a stationary mold [22]. Without rotation, no fluid motion was predicted during the early stages of solidification. However, in time, the density inversion induced by water enrichment of the liquid due to precipitation of NH_4Cl solid (dendritic crystals) became unstable and fluid motion was initiated. Instability was marked by perturbations in the liquid density and permeability along the liquidus front, which were, in turn, manifested by variations in the buoyancy force and the flow resistance of the mushy region. Irregularities in the growth of the liquidus front resulted from localized reductions in the liquidus temperature and were precursors to the nucleation of channels along the liquidus. The channels developed in the downward direction, providing preferred flow paths for cold, water-enriched fluid which ascended from the mushy region and appeared as buoyant plumes in the melt.

3.1. *Steady rotation*

As previously noted, experimental findings indicate that slow, steady rotation about the centerline during UDS has little effect on channel formation [27]. None the less, it is instructive to examine this condition as a baseline for assessing the effects of intermittent rotation.

For all simulations involving slow, steady rotation of the bounding surfaces of the computational domain, hydrodynamic conditions within the domain were characterized by a state of near solid-body rotation superimposed upon convective phenomena similar to those predicted in simulations without rotation. That is, solution of the continuum swirl equation yielded an angular momentum field which deviated only slightly from the solid-body state given by

$$\Omega = \Omega_s = \Omega_l = vr = \omega r^2. \tag{10}$$

Nevertheless, the liquid phase centripetal acceleration term in the radial momentum equation was obtained from the solution to equation (7). Although simulations were performed for several rotational speeds in the range from 10 to 120 rpm, differences were not significant, and the following discussion is limited to results obtained for rotation at 60 rpm.

During steady rotation of the system but prior to the onset of buoyancy induced convection, fluid motion can still be induced as a result of variations in the inertial body force. That is, the density inversion created by mushy zone solidification produces an *axial* density stratification which promotes *radial* flow due to an imbalance of the radial pressure gradient and the inertial force due to centripetal acceleration. The radial pressure gradient is established by the initial, imposed state of solid-body rotation and is balanced by the inertial body force based on the nominal density of the system. As solidification proceeds, strata of varying density develop in the mushy zone, with a corresponding variation in the centripetal force. For example, the density of interdendritic fluid is a minimum and a maximum near the cold boundary and the liquidus front, respectively. The inertial body force acting on fluid adjacent to the cold boundary is therefore less than that for overlying layers, and the net effect is an inwardly directed radial motion. In contrast, since the largest inertial force acts on dense fluid at the liquidus front, the fluid is centrifuged radially outward.

Figure 2 shows velocity vectors and isotherms in the bottom half of the mold for the time span during which the transition from inertial to buoyancy dominated convection occurs. After one minute of solidification, Fig. 2(a), the centrifuging effect is well-developed, with the majority of the mushy zone fluid being advected radially inward. However, at the liquidus front, the denser liquid flows toward the outer radius, while bulk liquid, possessing a downward component of motion, penetrates the liquidus to sustain the radial outflow. At the outer radius, the denser fluid bifurcates with part of the flow ascending along the outer wall and the other portion moving downward and then radially inward. Intrusion of the colder fluid into the bulk liquid is revealed by the isotherm near the liquidus front at the outer wall. Two minutes later, Fig. 2(b), hydrodynamic and thermal conditions are similar but the liquidus front is no longer planar near the outer wall. Cold fluid exiting the mushy zone is slightly depleted of solute (i.e. water-enriched), while the adjacent downflow of warmer, bulk fluid is at the initial composition. Differential diffusion rates of heat and solute sustain the fluid upflow at the outer wall, since the fluid gains thermal energy from the neighboring downflow of warmer fluid, while essentially retaining its composition. The strong downflow advects warmer fluid into the mush and inhibits freezing, even though its composition corresponds to the largest liquidus temperature.

The first evidence of channel formation occurs at $t \approx 5$ min, Fig. 2(c). Fluid moving radially outward along the liquidus is disrupted by inflow from the melt, and seeking a path of least resistance, it leaves the mushy zone before reaching the outer radius. Penetration of this cold fluid into the melt is revealed by

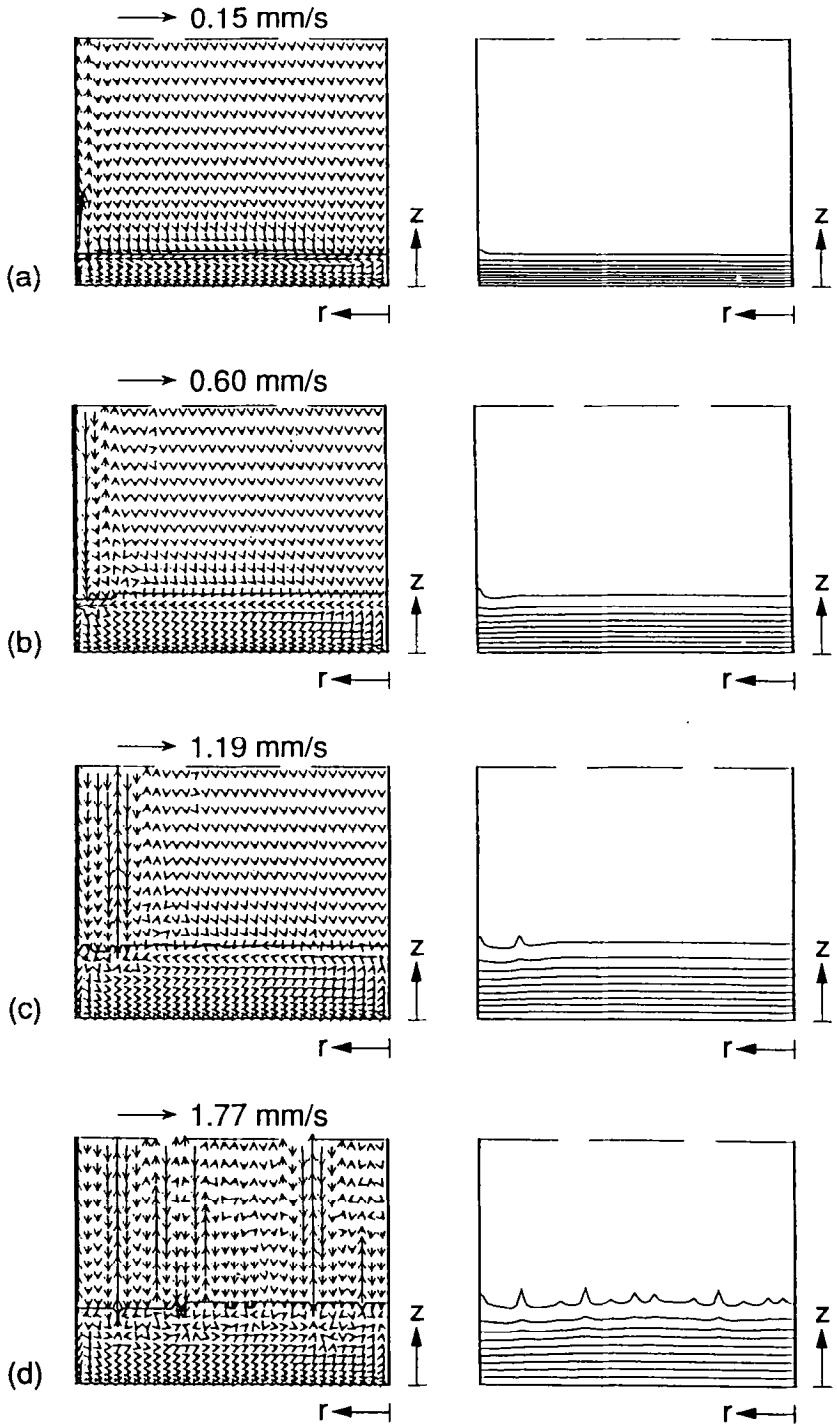

FIG. 2. Predicted velocity vectors and isotherms in the lower portion of the calculation domain for steady rotation at 60 rpm: (a) $t = 1$ min; (b) $t = 3$ min; (c) $t = 5$ min; (d) $t = 7$ min.

the isotherm at the liquidus front. The cold, solute depleted fluid remelts solid at the liquidus front creating a preferred flow path for neighboring interdendritic fluid. At this time buoyancy forces begin to influence fluid motion, and their effect is evident at other locations along the liquidus, where velocity vectors are no longer directed primarily in the downward direction. The effect is more pronounced near the centerline, since the centripetal force diminishes with decreasing radius.

Over the next two minutes, inertial and buoyancy forces are comparable. In much of the porous, dendritic

layer, the lighter fluid created by phase change continues to be centrifuged radially inward. However, near the more permeable liquidus front, the radial outflow predicted earlier is displaced by flow conditions conducive to channelling. That is, perturbations of density and permeability along the liquidus front induce local remelting, which is responsible for channel nucleation and an attendant solutally driven outflow of interdendritic fluid. At $t = 7$ min, Fig. 2(d), the effects of centrifuging are still evident by the direction of fluid flow in the bottom two-thirds of the mushy zone, but conditions near the liquidus resemble those of solidification without rotation [22]. For example, after penetrating the liquidus, fluid from the melt migrates to a channel, while fluid at the base of a channel exits the mushy region by ascending through the channel. As revealed by the isotherms, approximately eleven channels are developing. With increasing time, the transition from inertially dominated flow within the mush to one which is primarily governed by buoyancy effects continues to occur. As in the case of static solidification, the large number of channels which is predicted to occur initially decreases with increasing time. The remaining channels exhibit downward growth, as ascending fluid melts adjoining solid, creating preferred paths of flow.

Velocity vectors and streamlines, with the liquidus front superimposed, as well as isotherms and liquid isocomps, are presented in Fig. 3 for $t = 10$ min. The results may be compared with those presented in Fig. 11 of ref. [22] for equivalent conditions without rotation. The most striking difference is the effect that slow, steady rotation has on the flow field in the melt. Specifically, Figs. 3(a) and (b) reveal that motion associated with the buoyant plumes, which issue from five channels, is highly organized. The plumes ascend to the top of the domain, where bifurcation is followed by downflow to the liquidus. There is negligible mixing between adjoining plumes, with each plume sustaining elongated counter-rotating circulation cells. In contrast, although five plumes emanate from the liquidus for static solidification (Fig. 11 of ref. [22]), the plumes *meander* in the radial direction and experience considerable mutual interaction. Stabilization of the plumes, or their lack of meandering, is clearly evident in the streamlines of Fig. 3(b). Since shear forces are small, rotation has the effect of essentially striking a balance between the radial pressure gradient and the centripetal force. Radial and axial density variations, which contribute to variations in the centripetal force, are not large enough to promote a centrifuging effect in the melt. In addition, although shear forces between adjoining ascending and descending flows can induce radial motion, such motion is not sustainable due to the requirement that angular momentum must be conserved. Because density variations are small, a radially displaced particle of rotating fluid seeks to regain its original radial location in order to maintain a state of solid body rotation. Hence, superposition of a state of near solid-body rotation on a buoyancy-driven axial flow acts to suppress radial motion. The temperature and liquid composition fields at this time, Figs. 3(c) and (d), are nearly identical to those predicted for the static casting (Figs. 11(c) and (d) of ref. [22]).

Consistent with results obtained without rotation (Fig. 12 of ref. [22]), at $t = 19$ min, Fig. 4, three channels remain, with the outermost channel undergoing closure. Evidence of closure is revealed by downward fluid velocities within the channel and by the seepage of underlying interdendritic fluid into the neighboring channel, Fig. 4(a). The streamlines, Fig. 4(b), reveal a broadening in the radial extent of the recirculations associated with each plume, which may be due, at least in part, to the reduction in the number of channels from five at $t = 10$ min to three at $t = 19$ min. Relative to results for a static casting (Figs. 12(c) and (d) of ref. [22]), the temperature and to a greater extent the liquid composition contours of Figs. 4(c) and (d) confirm that the ascending plumes retain their thermal and solutal identities better in the presence of rotation.

In summary, consistent with the experimental observations of Sample and Hellawell [27], inertial effects produced by slow, steady rotation were insufficient to significantly alter the buoyancy forces responsible for localized remelting in the mushy zone. In particular, for rotational speeds up to 120 rpm, there was little difference in the time required for channels to develop, the number of channels, the physical mechanisms responsible for channel growth (or demise), and the associated development of thermosolutal plumes. Thus, aside from the centrifuging effect which occurs during the early stages of phase change and stabilization of the buoyancy plumes, the imposition of slow, steady rotation does not change the basic transport and solidification phenomena associated with static conditions.

3.2. *Intermittent rotation*

The response of a fluid-filled cavity to a time varying rotation is a fundamental hydrodynamic problem which has received considerable attention [33]. In the present study, the so-called spin-up problem [34] is considered. The problem pertains to the transient response of fluid contained in a cylindrical cavity as it seeks a final state of solid-body rotation, following an impulsive change in the angular frequency about the cavity centerline. It was first studied in detail by Wedemeyer [35], with variations on the theme investigated by many others, as, for example, Pearlstein [36] and Pedlosky [37].

The case of spin-up from rest may be used to illustrate the nature of the flow induced by rotation. Following the initial, impulsive change in the angular frequency, boundary layers, or so-called Ekman layers, begin to form on the bottom and top circular boundaries of the cavity. Angular momentum imparted via viscous effects to the fluid within these layers causes a centripetal force that results in outward

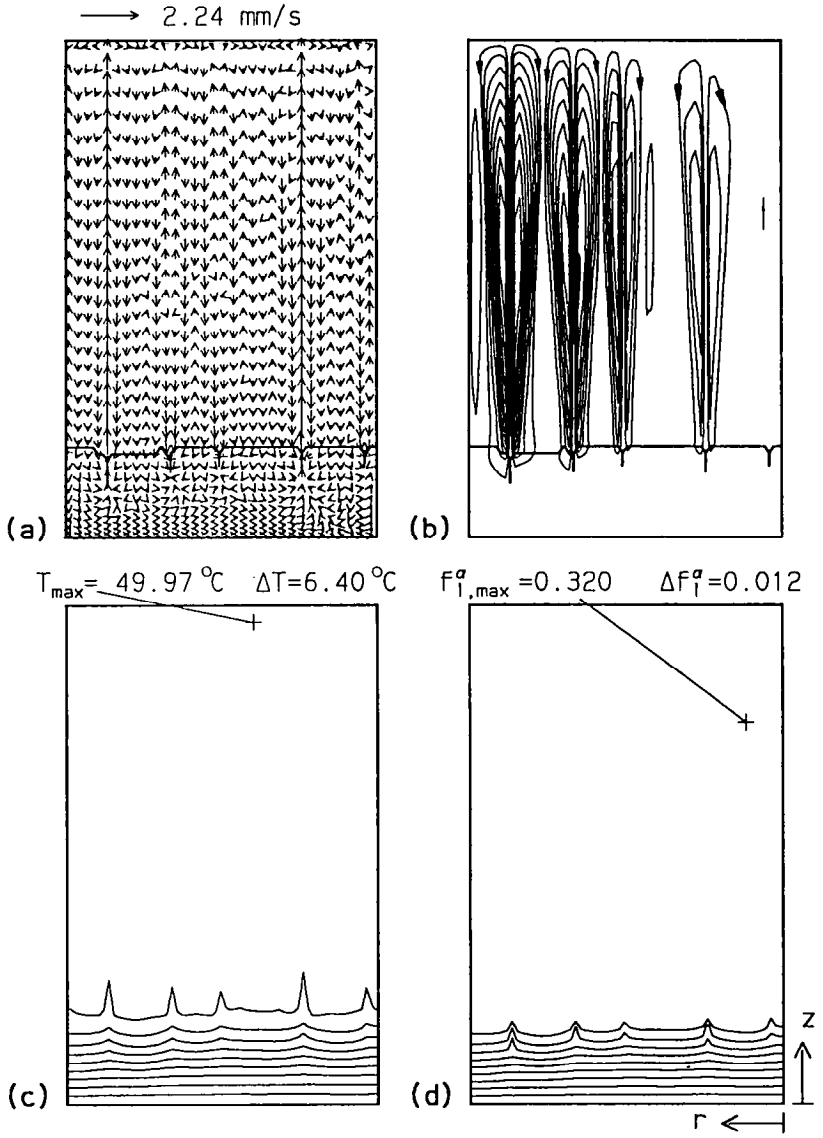

FIG. 3. Predicted solidification behavior at $t = 10$ min for steady rotation at 60 rpm: (a) velocity vectors; (b) streamlines; (c) isotherms; (d) liquid isocompositions.

radial flow. Conservation of mass requires that this transport be balanced by mass flow into the Ekman layers from the nearly quiescent core. Continuity also mandates weak, inwardly directed radial convection at the interior. During the early stages of spin-up, the interior or core flow that is directed radially inward to replace fluid entering the Ekman layers is essentially inviscid. A ring of fluid moving radially inward to sustain the Ekman flows must therefore conserve angular momentum, which is manifested by an increase in angular velocity with decreasing radial location. Hence, the Ekman layers act as sinks for low angular momentum fluid in the interior, with this fluid being replaced by higher angular momentum fluid drawn from larger radii [33]. Ultimately a steady state is achieved for which the Ekman boundary layers are no longer present and the system exhibits solid-body rotation. Greenspan [33] derived the following expression for the time required to attain solid-body rotation, the so-called spin-up time

$$\chi = \left(\frac{H^2}{\nu\omega}\right)^{1/2} = E^{-1/2}\omega^{-1} \tag{11}$$

where the Ekman number, $E = \nu/\omega H^2$, is a measure of the significance of viscous relative to rotational forces.

The process of spin-down is generally more complicated, since it leads to instability and possibly turbulence. If a system spinning in solid-body rotation is impulsively stopped, the angular momentum increases with decreasing radius, thereby disrupting the radial

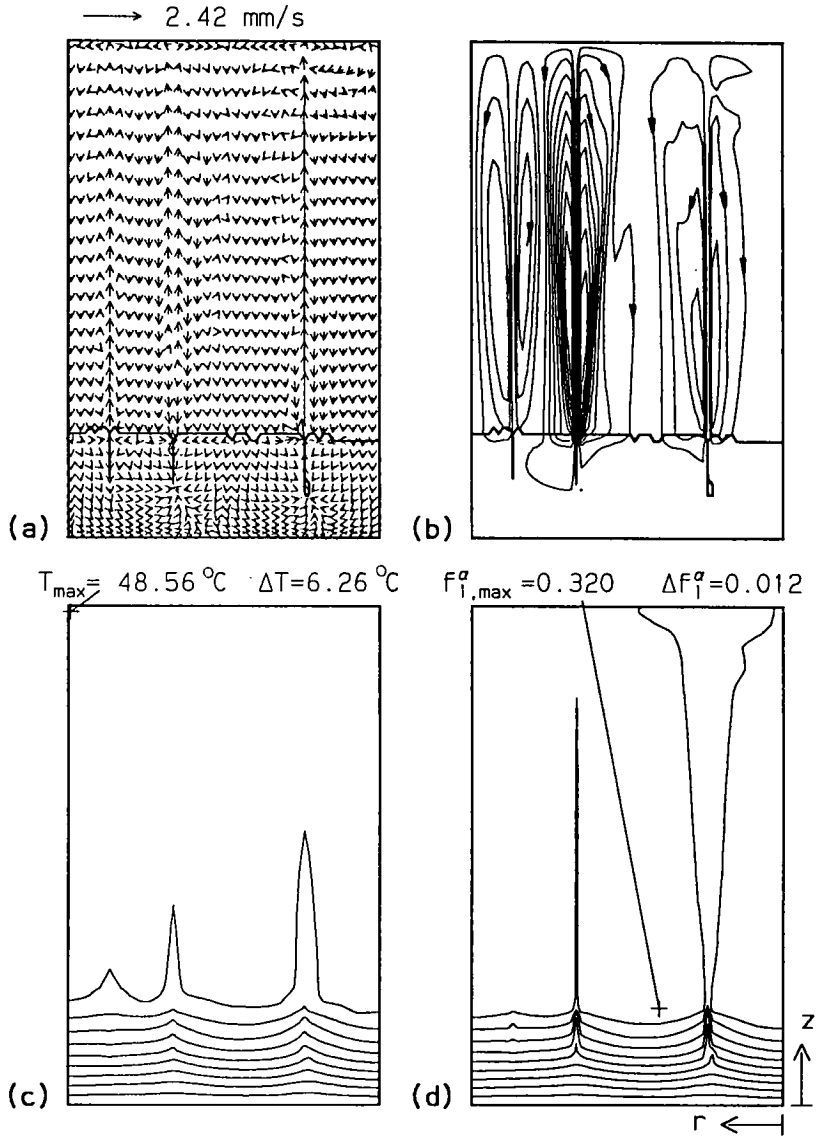

FIG. 4. Predicted solidification behavior at t = 19 min for steady rotation at 60 rpm: (a) velocity vectors; (b) streamlines; (c) isotherms; (d) liquid isocompositions.

pressure gradient. The condition of increasing angular momentum with decreasing radius occurs, for example, in Taylor–Couette flow [38].

The ultimate outcome of the spin-up process is a system which exhibits solid-body rotation. As revealed by the preceding calculations, such a condition has little effect on the prevention of channels. However, in the present study, it is the spin-up (and spin-down) process itself which is investigated to assess the potential for minimizing channel development caused by buoyancy driven flow. Since channels form at the liquidus front due to perturbations of the field variables affecting the density and permeability, the Ekman flow produced by spin-up and spin-down may be sufficient to 'wash' away the perturbations. Based on experimental findings for a steadily rotated UDS system that was tilted from the vertical, the 'washing' effect was suggested by Sample and Hellawell [27]. Because spin-up times are several orders of magnitude smaller than the time required for complete solidification, it is reasonable tc select an intermittency rate which corresponds to the theoretical spin-up time for the actual system. Thus, the system is spun-up to a condition of near solid-body rotation, whereupon spin-down is initiated by stopping the rotation of the bounding surfaces. Since the spin-down process is scaled similarly to spin-up, equivalent intervals of spin-down and spin-up represent a logical starting point for the study of solidification with intermittent rotation. For the present system, the theoretical spin-up time given by equation (10) is approximately 90 s for ω = 10 rpm. Although the

actual spin-up time is influenced by buoyancy and solidification effects, differences from the chosen value of 90 s are not critical to the intent of the simulation.

Figure 5 is a composite at $t = 10$ s of velocity vectors, streamlines, contours of constant angular momentum (all with the liquidus front superimposed), and isotherms. At $t = 0$, the swirl was specified along the bottom, top and outer surfaces according to $\Omega = \omega r^2$. The velocity field, Fig. 5(a), typifies the early stages of spin-up. Namely, viscous effects have imparted angular momentum to thin layers of fluid adjacent to the top surface and the liquidus front, and this fluid is driven radially outward due to the inertial force. At the outer wall, fluid in the Ekman layers turns and moves in the axial direction, ultimately meeting at $z \approx 0.4H$. Correspondingly, fluid which is removed from these layers and is not in close proximity to the outer wall slowly moves radially inward and upward/downward to feed the two Ekman layers.

The isoswirls in Fig. 5(c) have been normalized with the swirl of the outer wall, $\Omega|_{r_o} = \omega r_o^2$, and have been plotted in increments of 0.1. At this early stage of the spin-up process, fluid possessing angular momentum is confined to the Ekman layers and a region close to the outer radius, from which fluid is being 'flushed' by the spinning. The mushy region produces significant viscous drag, through the Darcian term in the swirl equation, to yield a mixture (continuum) swirl which is essentially equivalent to that of the solid phase. The swirl of the solid phase, Ω_s, is explicitly specified to be

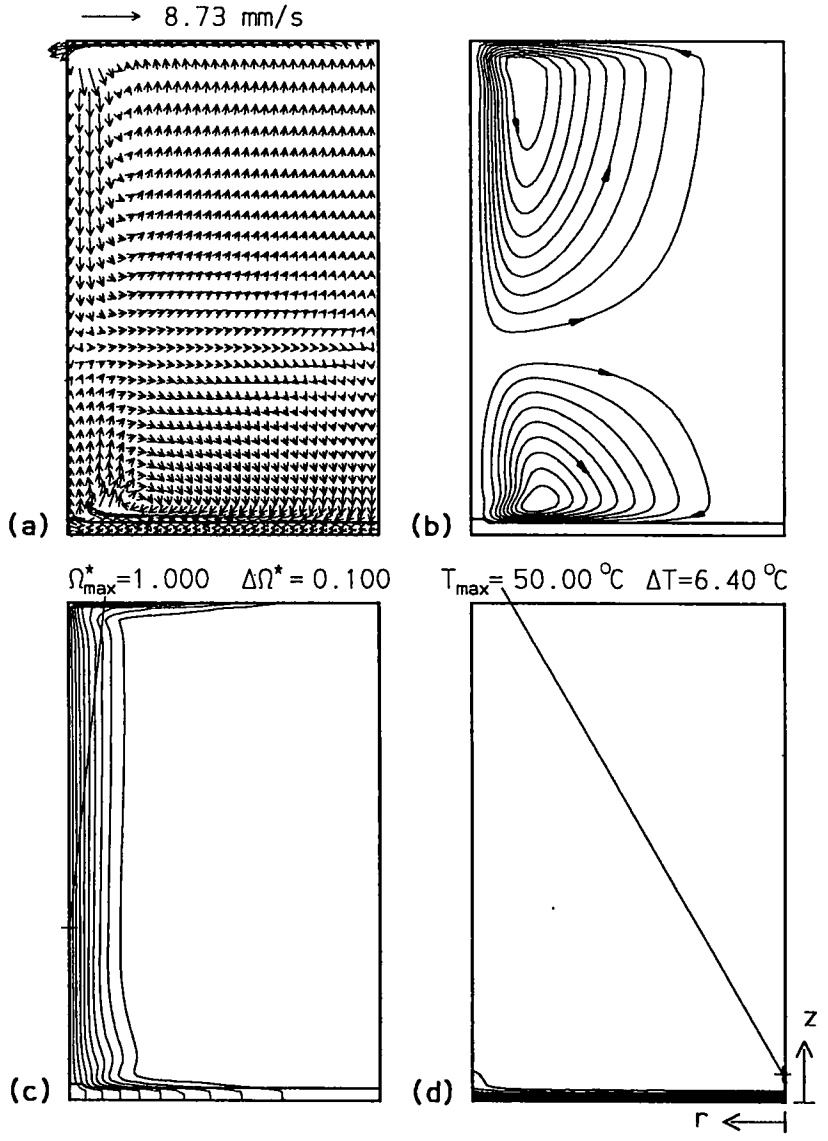

FIG. 5. Predicted solidification behavior at $t = 10$ s for spin-up at 10 rpm: (a) velocity vectors; (b) streamlines; (c) isoswirls; (d) isotherms.

equivalent to the boundary value at the radius of interest. That is, any solid which forms is assumed to rotate with the same angular frequency as the boundaries. Hence, with respect to angular momentum, the majority of the mushy zone acts as an extension of the bottom boundary, effectively reducing the height of the domain, and in turn, the theoretical spin-up time. Throughout the mushy zone, and particularly near the liquidus, the centripetal effect drives interdendritic fluid in the radial direction. This fluid is forced upward at r_0 and yields the cold spot revealed in the isotherms, Fig. 5(d).

At $t = 30$ s, the maximum velocity, Fig. 6(a), is reduced to approximately 80% of the value at $t = 10$ s, but still exceeds values typical for static solidification. The progression of spin-up is revealed by the increased spacing between isoswirls, Fig. 6(c), indicating that more of the inner core is beginning to rotate. Radial flow along the liquidus continues to promote localized cooling at the outer wall, Fig. 6(d), and hence greater solid formation at this location.

Field variables at the completion of the 90 s spin-up are shown in Fig. 7. The velocity vectors, Fig. 7(a), reveal vestiges of the Ekman layers, which are now sustained by upflow/downflow of core fluid moving at comparable velocities. A reduction in the maximum velocity to 27% of the value at $t = 10$ s is further evidence of the approach to solid-body rotation. The nearly vertical contours of the isoswirls at the larger radial locations, Fig. 7(c), indicate fluid movement with nearly the same angular velocity as the boundary. However, angular momentum gradients at the liqui-

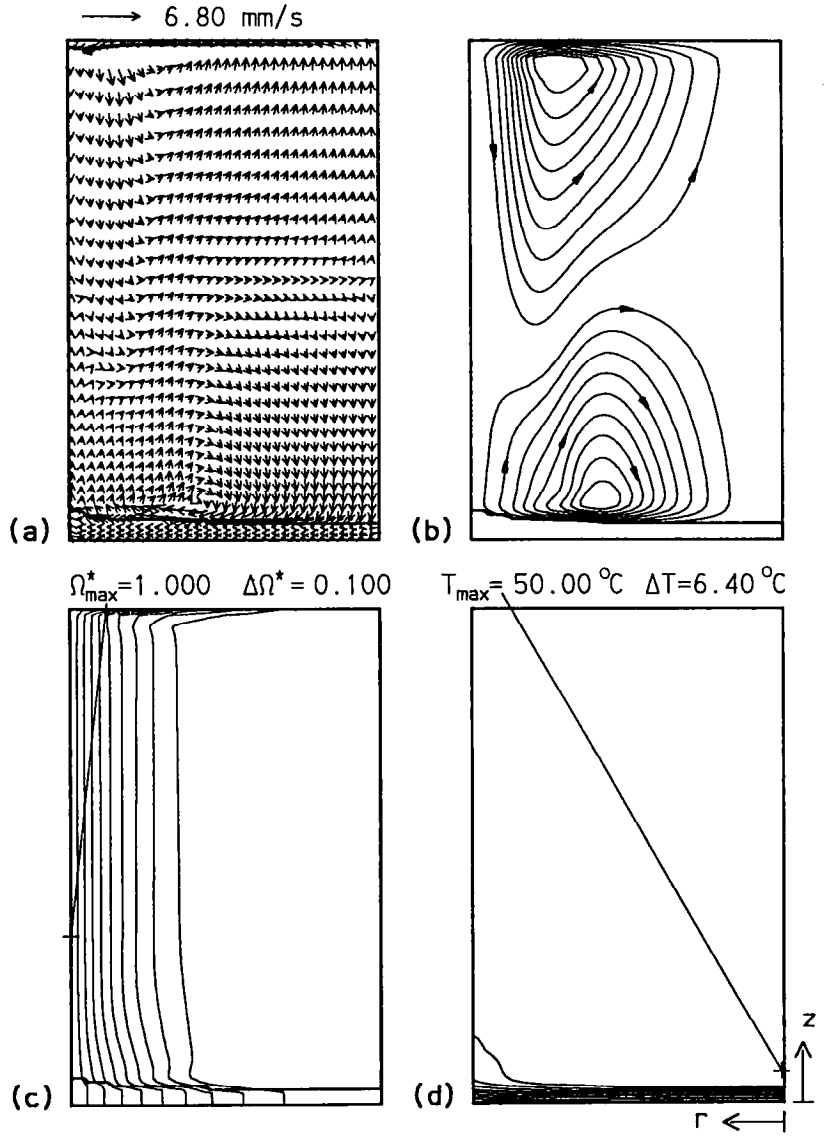

FIG. 6. Predicted solidification behavior at $t = 30$ s for spin-up at 10 rpm: (a) velocity vectors; (b) streamlines; (c) isoswirls; (d) isotherms.

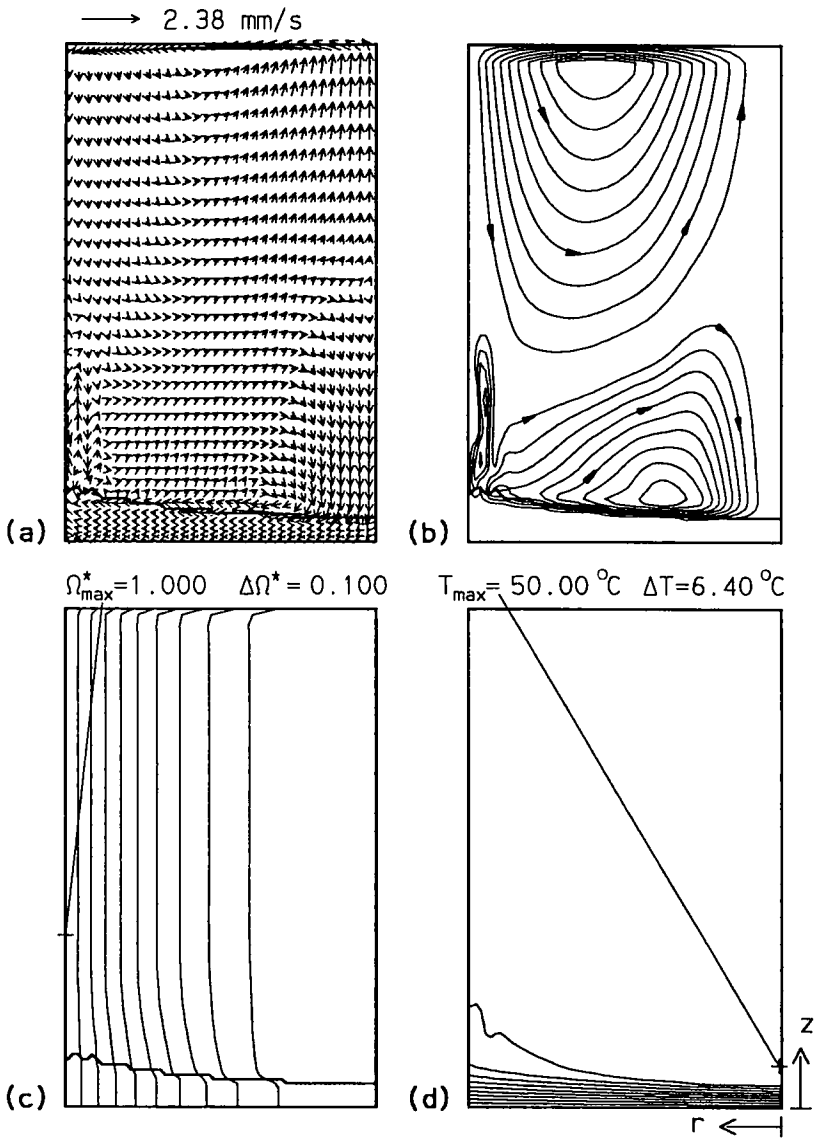

FIG. 7. Predicted solidification behavior at $t = 90$ s for spin-up at 10 rpm: (a) velocity vectors; (b) streamlines; (c) isoswirls; (d) isotherms.

dus front and the top boundary for radial positions closer to the centerline imply that spin-up has not yet been attained. The isotherms, Fig. 7(d), exhibit a pronounced upward deflection at r_0, which corresponds to increasing mushy zone thickness with increasing radius. The maximum temperature, which is equivalent to T_0, continues to exist near the centerline and liquidus front and is a manifestation of warm, core fluid drawn to the bottom Ekman layer.

Ten seconds after the cessation of imposed spinning, the velocity field, Fig. 8(a), is dominated by a strong, clockwise flow in the bottom-half of the domain. Flow in the mushy zone is directed radially outward, as it was during the spin-up interval, and flow in the top portion of the cavity is characterized by continued existence of the Ekman layer, Fig. 8(b). However, due to the diffusion of viscous effects from the boundaries, adjoining fluid begins to lose angular momentum, Fig. 8(c), immediately after rotation is stopped. For example, the angular momentum of fluid near the outer radius becomes equivalent to that of core fluid closer to the centerline, resulting in closure of the swirl contours. At this time, the maximum swirl is approximately 61% of the value imposed at the outer boundary during rotation. Its internal location, as well as the pronounced swirl gradients above the liquidus front, yield significant spatial variations in the centripetal force. The temperature field, Fig. 8(d), is influenced by the strong radial flow of warmer, core fluid above the liquidus, which promotes a more horizontal distribution of isotherms than that existing at the end of the spin-up, Fig. 7(d).

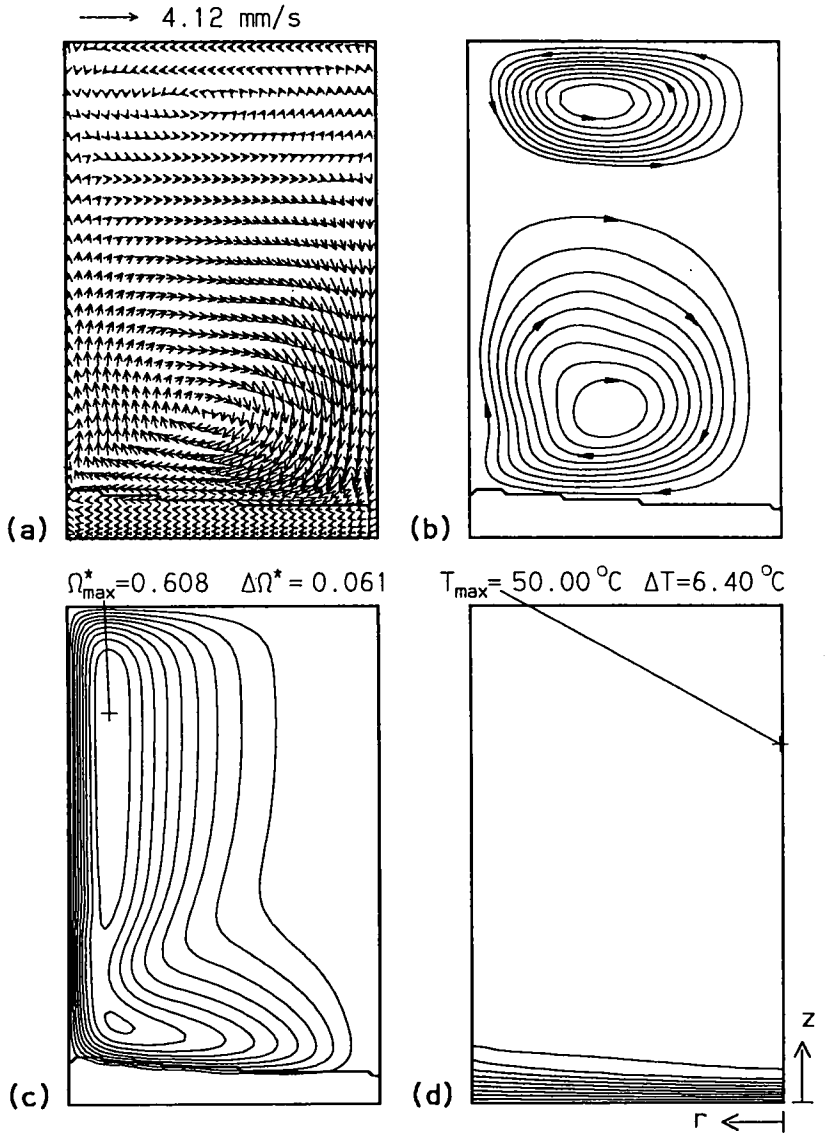

FIG. 8. Predicted solidification behavior at t = 100 s for spin-down (zero rotation): (a) velocity vectors; (b) streamlines; (c) isoswirls; (d) isotherms.

The dynamic response of the system to spin-down is further illustrated in Fig. 9 for t = 130 s, which is 40 s after imposed rotation was stopped. Conditions in the interval $90 \leqslant t \leqslant 130$ s revealed an oscillation in the direction of radial flow at the liquidus front. Although flow at the interface was directed outward at 90 s, Fig. 8(a), successive reversals in this direction occurred at $t \approx 110$ and 120 s (not shown). At t = 130 s, Figs. 9(a) and (b), a strong radial outflow exists slightly above the liquidus and contributes to a recirculation which drives flow radially inward along the liquidus. Additional recirculation zones within the melt also arise from spatially varying values of the centripetal force, as indicated by the angular momentum field, Fig. 9(c).

Radial inflow predicted along the liquidus front at t = 130 s persists for the remainder of the spin-down interval. At t = 180 s, which corresponds to completion of the first spin-down cycle, the flow field, Figs. 10(a) and (b), is characterized by two recirculation cells which divide the computational domain at the approximate mid-height. This condition is linked to the angular momentum field, Fig. 10(c), which is related to the variation of the centripetal force term in the radial momentum equation. Expressing the liquid phase centripetal acceleration of equation (2) in terms of the liquid phase swirl

$$\frac{v_l^2}{r} = \frac{\Omega_l^2}{r^3} \tag{12}$$

it follows that the point of maximum angular momen-

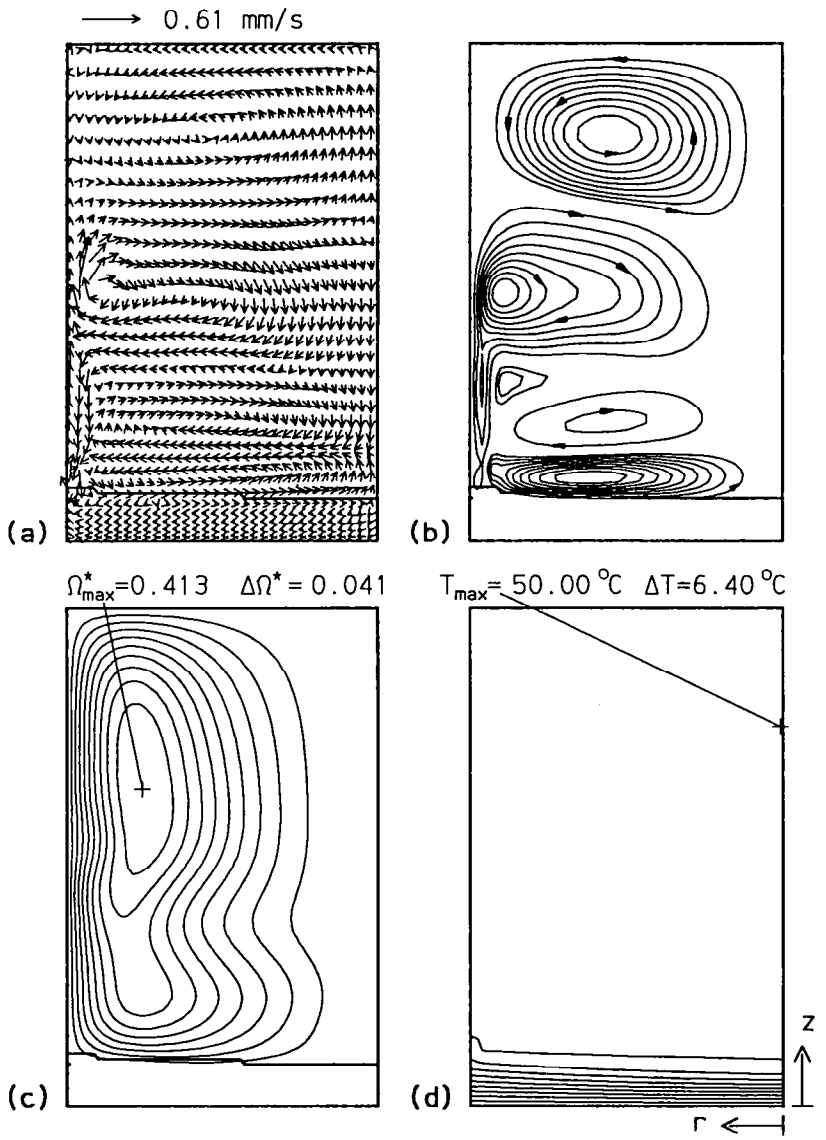

FIG. 9. Predicted solidification behavior at t = 130 s for spin-down (zero rotation): (a) velocity vectors; (b) streamlines; (c) isoswirls; (d) isotherms.

tum shown in Fig. 10(c) corresponds approximately to the location of maximum inertial force. The strong radial outflow at $z \approx 0.5H$, Figs. 9 and 10, is a manifestation of this maximum. With the exception of the cold spots at the liquidus near the centerline and outer radius, the isotherms in Fig. 10(d) are essentially horizontal, implying diffusion-dominated phase change.

Conditions for subsequent spin-up and spin-down cycles are similar to those associated with the initial interval of intermittent rotation. The most noteworthy feature of the second intermittent rotation cycle is the onset of localized remelting. After $t \approx 4$ min, a channel nucleates at the junction of the liquidus front with the outer wall. During the spin-down process of the third interval ($t \approx 8$ min), nucleation of a second channel occurs at the centerline.

Contrasting conditions at t = 19 min, Fig. 11, with those previously obtained for static solidification, it is evident that the imposed, time-varying rotation has a significant effect on channel development. Without rotation, three channels are dispersed within the core of the casting (Fig. 12 of ref. [22]), while Fig. 11(a) reveals the existence of two channels at the extremities of the casting (the centerline and outer radius). A spin-up cycle is occurring at this time, and its effects are superimposed on the thermosolutally driven flows exiting the two channels. The related mixed convection effect is most evident at the outer radius, where the developing Ekman layers interact with fluid ascending from the channel, Figs. 11(a) and (b). Penetration of both channels into the mushy region significantly exceeds that predicted for static solidi-

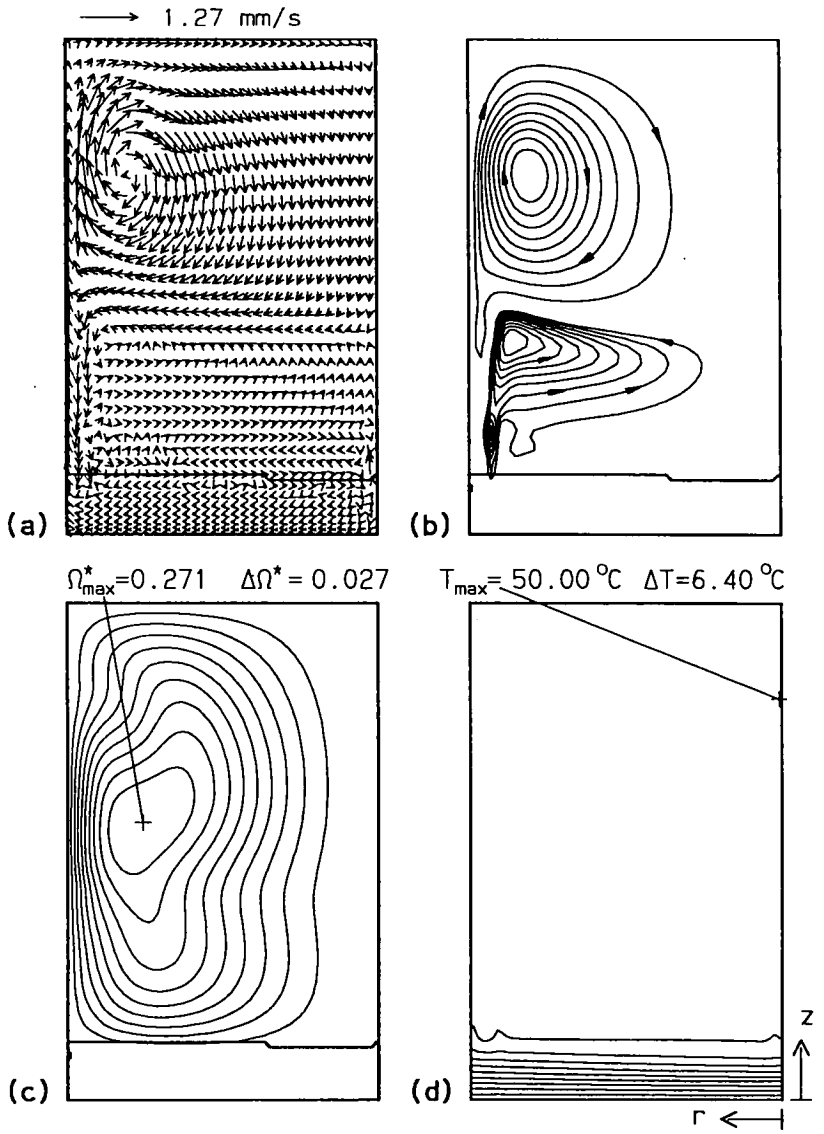

FIG. 10. Predicted solidification behavior at t = 180 s for spin-down (zero rotation): (a) velocity vectors; (b) streamlines; (c) isoswirls; (d) isotherms.

fication, suggesting that remelting is more effective for intermittent rotation, particularly at r_0, since cold, solute-depleted fluid within the mush is continuously driven in the positive radial direction by centripetal effects. The total fraction of solid formed after 19 min is 2.2%, which is essentially the same as that for static solidification.

4. SUMMARY

Despite its geometrical simplicity, alloy casting by means of unidirectional solidification (UDS) is characterized by complex and strongly coupled transport phenomena occurring in the liquid (melt) and solid/liquid (mushy) regions which exist during solidification. In static solidification, an unfortunate consequence of this transport is the establishment of large compositional variations, and hence severe defects, in the final casting. The process responsible for formation of the defects is known as macrosegregation, and in the case of UDS, it is manifested by negative segregation and pencil-like freckles, that is, vertically aligned regions of nearly eutectic composition that are distributed randomly across the casting. In a recent numerical simulation [22], it was definitively established that freckles originate from flow channels that nucleate at the liquidus front. Nucleation results from perturbations in field variables which influence the local density and permeability, such that attendant remelting fosters downward propagation of the channels into the mushy region.

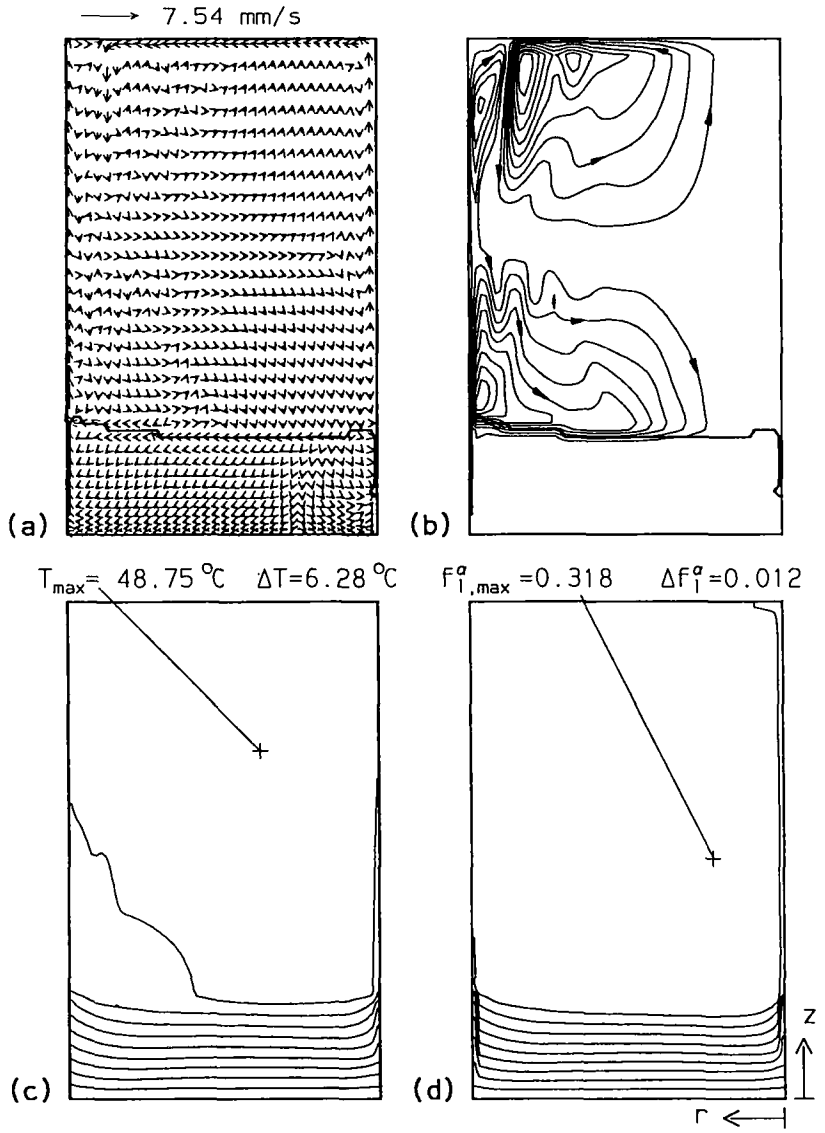

FIG. 11. Predicted solidification behavior at $t = 19$ min (during spin-up for the seventh cycle of the intermittent rotation process): (a) velocity vectors; (b) streamlines; (c) isotherms; (d) liquid isocompositions.

From an experimental study of UDS in a cylindrical mold which was steadily rotated and tilted about the vertical axis [27], it was surmised that perturbations at the liquidus front and subsequent channel formation could be inhibited by *washing* the front with a radially induced flow. The objective of this study was to assess this premise by numerically simulating solidification in a cylindrical mold with both steady and intermittent rotation.

Simulations were performed for solidification of a hypereutectic NH_4Cl solution ($f_0^{NH_4Cl} > f_e^{NH_4Cl}$) at rotational speeds up to 120 rpm. For steady rotation, channels were predicted to develop in much the same manner as for static solidification, and apart from stabilization of the buoyant plumes emanating from the channels, the imposed rotation had little effect on basic transport and solidification phenomena. However, for slow, intermittent rotation, which corresponded to successive *spin-up* and *spin-down* of the system over a time interval much less than that required for complete solidification, significant beneficial effects were predicted. Namely, following an initial impulsive change in angular frequency associated with spin-up, the liquidus front was washed by an Ekman boundary layer and channel nucleation was preempted in core regions of the casting. Although channels subsequently developed at the centerline and the outer radius of the casting, both locations correspond to regions where freckles could be readily removed through post-processing of the casting.

The foregoing results suggest that, with respect to chemical homogeneity, the quality of unidirectionally solidified binary alloys may be enhanced through intermittent rotation of the mold. By restricting freckling to the centerline and outer radius of the casting, active control of UDS in this manner would yield an ingot which is predominantly free of significant defects.

Acknowledgements—Support of this work by the U.S. Department of Energy under Award Number DE-FG02-87ER13759 is gratefully acknowledged.

REFERENCES

1. H. E. Huppert, The fluid mechanics of solidification, *J. Fluid Mech.* **212,** 209–240 (1990).
2. K. M. Fisher, The effects of fluid flow on the solidification of industrial castings and ingots, *PhysicoChem. Hydrodyn.* **2,** 311–326 (1981).
3. C. F. Chen and F. Chen, Experimental study of directional solidification of aqueous ammonium chloride solution, *J. Fluid Mech.* **227,** 567–586 (1991).
4. S. M. Copley, A. F. Giamei, S. M. Johnson and M. F. Hornbecker, The origin of freckles in unidirectionally solidified castings, *Met. Trans.* **1,** 2193–2204 (1970).
5. A. F. Giamei and B. H. Kear, On the nature of freckles in nickel base superalloys, *Met. Trans.* **1,** 2185–2192 (1970).
6. W. W. Mullins and R. F. Sekerka, Stability of a planar interface during solidification of a dilute binary alloy, *J. Appl. Phys.* **35,** 444–451 (1964).
7. S. R. Coriell, M. R. Cordes, W. J. Boettinger and R. F. Sekerka, Convective and interfacial instabilities during unidirectional solidification of a binary alloy, *J. Crystal Growth* **44,** 13–28 (1980).
8. G. B. McFadden, R. G. Rehm, S. R. Coriell, W. Chuck and K. A. Morrish, Thermosolutal convection during dendritic solidification, *Met. Trans. A* **15A,** 2125–2137 (1984).
9. D. R. Jenkins, Nonlinear analysis of convective and morphological instability during solidification of a dilute binary alloy, *PhysicoChem. Hydrodyn.* **6,** 521–537 (1985).
10. A. C. Fowler, The formation of freckles in binary alloys, *IMA J. Appl. Math.* **35,** 159–174 (1985).
11. P. Nandapurkar, D. R. Poirier, J. C. Heinrich and S. Felicelli, Thermosolutal convection during dendritic solidification of alloys: Part I. Linear stability analysis, *Met. Trans. B* **20B,** 711–721 (1989).
12. J. C. Heinrich, S. Felicelli, P. Nandapurkar and D. R. Poirier, Thermosolutal convection during dendritic solidification of alloys: Part II. Nonlinear convection, *Met. Trans. B* **20B,** 883–891 (1989).
13. M. G. Worster, Structure of a convecting mushy layer, *Appl. Mech. Rev.* **43**(2), S59–S62 (1990).
14. W. D. Bennon and F. P. Incropera, A continuum model for momentum, heat and species transport in binary solid–liquid phase change systems: I. Model formulation, *Int. J. Heat Mass Transfer* **30,** 2161–2170 (1987).
15. V. Voller and C. Prakash, A fixed grid numerical modelling methodology for convection–diffusion mushy region phase-change problems, *Int. J. Heat Mass Transfer* **30,** 1709–1719 (1987).
16. C. Beckermann and R. Viskanta, Double-diffusive convection during dendritic solidification of a binary mixture, *PhysicoChem. Hydrodyn.* **10,** 195–213 (1988).
17. S. Ganesan and D. R. Poirier, Conservation of mass and momentum for the flow of interdendritic liquid during solidification, *Met. Trans. B* **21B,** 173–181 (1990).
18. P. J. Prescott, F. P. Incropera and W. D. Bennon, Modeling of dendritic solidification systems: reassessment of the continuum momentum equation, *Int. J. Heat Mass Transfer* **34,** 2351–2359 (1991).
19. W. D. Bennon and F. P. Incropera, A continuum model for momentum, heat and species transport in binary solid–liquid phase change systems: II. Application to solidification in a rectangular cavity, *Int. J. Heat Mass Transfer* **30,** 2171–2187 (1987).
20. W. D. Bennon and F. P. Incropera, The evolution of macrosegregation in statically cast binary ingots, *Met. Trans. B* **18B,** 611–616 (1987).
21. M. C. Christenson, W. D. Bennon and F. P. Incropera, Solidification of an aqueous ammonium chloride solution in a rectangular cavity—II. Comparison of predicted and measured results, *Int. J. Heat Mass Transfer* **32,** 69–79 (1989).
22. D. G. Neilson and F. P. Incropera, Unidirectional solidification of a binary alloy and the effects of induced fluid motion, *Int. J. Heat Mass Transfer* **34,** 1717–1732 (1991).
23. D. G. Neilson, Unidirectional solidification of a binary model alloy and the effects of induced fluid motion, Ph.D. Thesis, Purdue University (1991).
24. D. G. Neilson and F. P. Incropera, Three-dimensional considerations of unidirectional solidification in a binary mixture, *Numer. Heat Transfer* (in press).
25. M. H. McCay and T. D. McCay, Experimental measurement of solutal layers in unidirectional solidification, *J. Thermophysics* **2,** 197–202 (1988).
26. A. K. Sample and A. Hellawell, The effect of mold precession on channel and macro-segregation in ammonium chloride–water analog castings, *Met. Trans. B* **13B,** 495–501 (1982).
27. A. K. Sample and A. Hellawell, The mechanisms of formation and prevention of channel segregation during alloy solidification, *Met. Trans. A* **15,** 2163–2173 (1984).
28. W. E. Langlois, Conservative differencing procedures for rotationally symmetric flow with swirl, *Comput. Meth. Appl. Mech. Engng* **25,** 315–333 (1981).
29. W. E. Langlois, Buoyancy-driven flows in crystal-growth melts, *Ann. Rev. Fluid Mech.* **17,** 191–215 (1985).
30. W. D. Bennon and F. P. Incropera, Numerical analysis of binary solid–liquid phase change using a continuum model, *Numer. Heat Transfer* **13,** 277–296 (1988).
31. S. Asai and I. Muchi, Theoretical analysis and model experiments on the formation mechanism of channel-type segregation, *Trans. ISIJ* **18,** 90–98 (1978).
32. S. V. Patankar, *Numerical Heat Transfer and Fluid Flow.* Hemisphere, Washington, DC (1980).
33. H. P. Greenspan, *The Theory of Rotating Fluids.* Cambridge University Press, Cambridge (1968).
34. E. R. Benton and A. Clark, Jr., Spin-up, *Ann. Rev. Fluid Mech.* **6,** 257–280 (1974).
35. E. H. Wedemeyer, The unsteady flow within a spinning cylinder, *J. Fluid Mech.* **20**(3), 383–399 (1964).
36. A. J. Pearlstein, Effect of rotation on the stability of a doubly diffusive fluid layer, *J. Fluid Mech.* **103,** 389–412 (1981).
37. J. Pedlosky, The spin-up of a stratified fluid, *J. Fluid Mech.* **28**(3), 463–479 (1967).
38. H. Schlichting, *Boundary Layer Theory,* 7th edn. McGraw-Hill, New York (1979).